

Article

Experimental and Physico-Chemical Comparison of ZnO Nanoparticles' Activity for Photocatalytic Applications in Wastewater Treatment

Stefano Alberti * , Irene Basciu, Marco Vocciante  and Maurizio Ferretti 

Department of Chemistry and Industrial Chemistry, University of Genoa, Via Dodecaneso 31, 16146 Genoa, Italy; irene.basciu55@gmail.com (I.B.); marco.vocciante@unige.it (M.V.); ferretti@chimica.unige.it (M.F.)

* Correspondence: stefano.alberti@edu.unige.it; Tel.: +39-010-3358737

Abstract: In this contribution, the photoactivity upon activation by simulated sunlight of zinc oxide (ZnO) obtained from two different synthetic pathways (Acetate and Nitrate) is investigated for water purification. Different reagents and processes were exploited to obtain ZnO nanoparticles. Products have been characterized by means of X-Ray Diffraction, Scanning Electron Microscopy along with Energy Dispersive Spectrometer, Dynamic Light Scattering, and Diffuse Reflectance Measurements, to highlight the different outcomes ascribable to each synthesis. A comparison of characteristics and performances was also carried out with respect to commercial ZnO. Nanoparticles of this semiconductor can be obtained as aggregates with different degrees of purity, porosity, and shape, and their physical-chemical properties have been addressed to the specific use in wastewater treatment, testing their effectiveness on the photocatalytic degradation of methylene blue (MB) as a model pollutant. Excluding the commercial sample, experimental results evidenced a better photocatalytic behavior for the ZnO Nitrate sample annealed at 500 °C, which was found to be pure and stable in water, suggesting that ZnO could be effectively exploited as a heterogeneous photocatalyst for the degradation of emerging pollutants in water, provided that thermal treatment is included in the synthetic process.

Keywords: zinc oxide; nanoparticle synthesis; photocatalysis; wastewater treatment; emerging pollutants removal; advanced oxidation processes



Citation: Alberti, S.; Basciu, I.; Vocciante, M.; Ferretti, M. Experimental and Physico-Chemical Comparison of ZnO Nanoparticles' Activity for Photocatalytic Applications in Wastewater Treatment. *Catalysts* **2021**, *11*, 678. <https://doi.org/10.3390/catal11060678>

Academic Editors: Gassan Hodaifa, Rafael Borja and Weilin Dai

Received: 26 February 2021
Accepted: 24 May 2021
Published: 26 May 2021

Publisher's Note: MDPI stays neutral with regard to jurisdictional claims in published maps and institutional affiliations.



Copyright: © 2021 by the authors. Licensee MDPI, Basel, Switzerland. This article is an open access article distributed under the terms and conditions of the Creative Commons Attribution (CC BY) license (<https://creativecommons.org/licenses/by/4.0/>).

1. Introduction

Environmental pollution represents a severe threat to the health of all living beings due to the presence of thousands of hazardous compounds continuously released into the environment as a consequence of various industries, such as pharmaceutical, cosmetic, plastic, leather, and textile [1]. Many of these pollutants are chemically stable, so they can accumulate and spread over a wide variety of processes in water and soil. The presence of such toxic and non-biodegradable molecules has drastically reduced the quality of the environment, causing toxicity to aquatic life, carcinogenicity to humans, and many other insidious side effects [2].

It is well evident that there is an urge to find effective and eco-sustainable methodologies able to counteract the spread of environmental pollution and its related drawbacks. Nowadays, several treatment methods such as biodegradation, adsorption, flocculation, and coagulation can be used to face different types of contamination in a practical way; adsorption-based technologies, in particular, are known to be a simple and cost-effective approach for the removal of various contaminants, both organic [3] and inorganic, such as metals [4] and nitrogen compounds [5], relying on a remarkable variety of adsorbent materials, which also includes the reuse of some industrial waste [6].

However, in most cases, these conventional approaches are not effective enough to achieve complete removal of pollutants from waters [7]. Therefore, in recent years, scientific research focused on innovative and powerful methods known as Advanced

Oxidation Processes (AOPs), to both increase the oxidation of recalcitrant pollutants and allow the simultaneous removal of a large variety of compounds. All AOPs are based on the generation of Reactive Oxygen Species (ROS), which are very reactive radical species that behave as powerful oxidants, and of all ROS, the hydroxyl radical is known to be the most powerful oxidizing agent for degrading non-biodegradable compounds as well as hazardous microorganisms in the aqueous phase. In addition, if AOPs are compared to other commonly used decontamination processes, the formation of the main disinfection by-products is not involved in such methods, making it possible to extend their application to drinking water facilities.

Being an eco-sustainable process, which involves the generation of hydroxyl radicals, heterogeneous semiconductor photocatalysis is considered a promising approach among AOPs. After the absorption of either artificial or natural light (as Grotthuss–Draper law states) by a semiconductor metal oxide, e.g., ZnO and/or TiO₂, the promotion of an electron within the semiconductor's electronic bands results in the formation of the radical (upon reaction with a water molecule, for instance); subsequently, the total mineralization of refractory organic compounds is promoted [8,9]. Nano-sized semiconductor metal oxides are considered efficient for their large surface area, low cost, long lifespan, excellent chemical as well as thermal stability, and low toxicity. Over the past few decades, nanomaterials have emerged as promising commodities in many fields including cosmetics, healthcare, biomedicine, food and feed, drug-delivery, the environment, catalysis, electronics, the space industry, energy science, optics, and light emitters [10,11]. However, properties and potential applications of nanoparticles vary with their phases, sizes, and morphologies, so the synthesis of such materials plays a fundamental role in the optimization of these metal oxides according to the specific purpose to fulfill.

Among all photocatalysts, ZnO is of great interest due to a plethora of interesting features: it is a semiconductor with a wide direct band gap (3.37 eV) [12] that is also non-toxic, highly photo-sensitive, physicochemically stable, environmentally friendly, and bio-compatible. Therefore, it can be effectively used in many applications such as catalysis, piezoelectric devices, chemical sensors, solar cells, antireflection coatings, sunscreen, antimicrobial agents, and so on [13], with its properties being strongly dependent on the method by which it is prepared [14].

Currently, several synthetic pathways are available: Laser ablation, hydrothermal synthesis, co-precipitation, gas or vapor transport, and pressurized melt-blow [15] are some of the options. Generally, bottom-up and top-down techniques are the two major processes used to synthesize nanoparticles, such as redox practices [16] and sol-gel processing, which guarantee easy, low cost, and homogeneous products, and enhance the control of the chemical composition with good reproducibility [17–20]. However, compared to other approaches, soft chemistry routes give the possibility to investigate the synthesis of new photocatalytic materials by merging different active agents in different steps of the synthesis. Indeed, the coupling of different materials in composite photocatalysts showing increased performances is widely reported in the literature [21–24]. In most cases, this is also a much simpler approach than trying to adapt commercially available products to specific needs. Several zinc precursors may be used for the synthesis: nitrate, chloride, perchlorate, acetylacetonate, propoxide, acetate, but metal salts are reported to be more suitable for large-scale production. The synthesis of ZnO nanoparticles can also be considered taking innovative and green synthetic routes into account: plant extracts [25], green tea leaves [26], honey [27], aloe bardanensis leaves, brown marine macroalgae [28], Arabic gum [29] and starch [30] are some examples of chemical's green sources. Unfortunately, the main drawbacks are related to the presence of impurities and disadvantageous microstructures in the final products, which are likely to hinder the photocatalytic activity of the semiconductor [31,32]. Post-treatments improve the crystalline quality without reducing photoactive defects [33,34]; some research papers, for example, report innovative synthetic routes able to lower the post-treatment temperature for the crystalline phase using nanoparticles as nucleation seeds [35,36].

From what has been said, ZnO activity is closely related to the morphology and shape of nanoparticles, including their microstructural and surface features, which is, in turn, the function of the annealing procedure [37]. In particular, the Wurtzite crystalline habitus is widely reported to be the most thermodynamically stable and favorable for photocatalytic processes [38].

Given this, this work aims to experimentally investigate the characteristics and performances of ZnO photocatalysts obtained by employing two distinct synthetic paths retrieved from known literature, in comparison with a commercial ZnO catalyst. Such synthesis paths were selected as they involve chemical reagents of different natures and different post-treatment processes (presence and absence of an annealing treatment), making it possible to correlate the outcomes of the investigated routes with the final physico-chemical and morphological features of Wurtzite ZnO NPs.

The photocatalytic activity of the samples was also preliminarily evaluated over the degradation of methylene blue solutions, to get insights on the applicability in the wider field of wastewater remediation. Indeed, a further key aspect is that synthetic paths considered are suitable for easy self-production, possibly recovering resources from waste materials, which represents added value in terms of environmental sustainability if compared to brand-new commercial products being specifically purchased.

2. Results and Discussion

2.1. Physico-Chemical Characterization

Figure 1 shows the XRD spectra of the synthesized ZnO samples, compared to the Wurtzite ZnO reference.

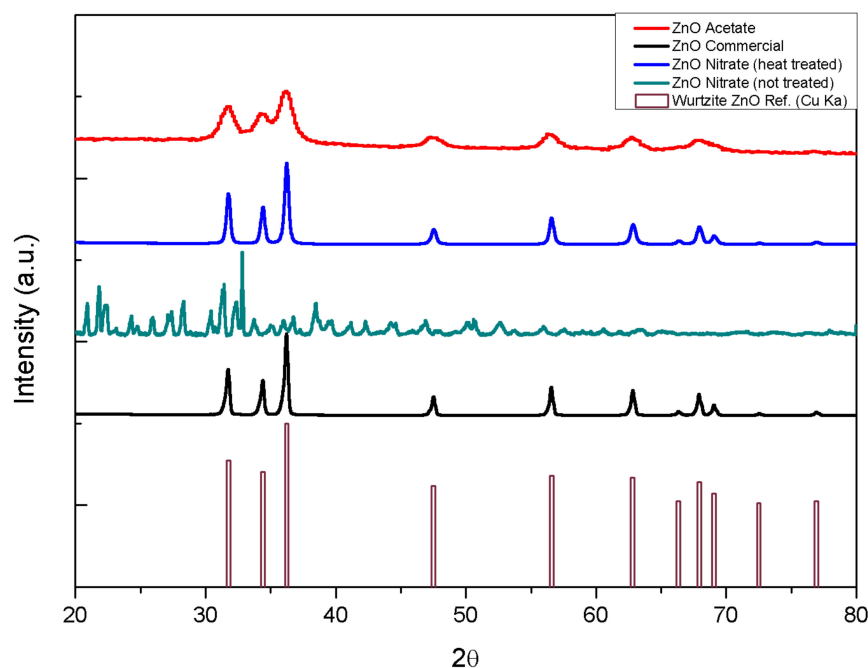


Figure 1. XRD experimental spectra obtained from synthesized samples compared to ZnO hexagonal Wurtzite reference spectrum (retrieved from Pearson's Crystal Data database, n° 1837628).

In Figure 1, as well as throughout the manuscript, the ZnO Acetate label refers to the ZnO sample obtained from the acetate route, while ZnO Nitrate labels refer to the ZnO samples obtained from the Nitrate route, as described in Section 3.1. Based on XRD measurements, it was possible to confirm that the untreated ZnO Nitrate sample is ascribable to unreacted $Zn_3(C_6H_5O_7)_2 \cdot 7H_2O$, as typical peaks belonging to the hexagonal Wurtzite phase are completely absent, in favor of a more complicated XRD pattern. As highlighted in Section 3.1.1, the lack of thermal treatment did not allow the finished ZnO product to be obtained (Equation (2)), with the synthesis stopping at the Zinc citrate

intermediate step. For what concerns other synthesized samples, it is possible to state that both the Citrate and Nitrate (heat-treated) synthetic paths led to the same outcome in terms of the crystalline hexagonal Wurtzite phase (reported for reference).

From the Person Crystal Database comparison, it was possible to assign the correct Miller index values to the crystallographic peaks: (100) to $31.73 2\theta$; (002) to $34.39 2\theta$; (101) to $36.20 2\theta$; (102) to $47.49 2\theta$; (110) to $56.54 2\theta$; (103) to $62.80 2\theta$; (200) to $66.34 2\theta$; (112) to $67.90 2\theta$; and (201) to $69.04 2\theta$. In this case, the crystalline outcome did not remarkably change according to the different synthetic paths, so it seems that the acetate route could be advantageously used to get Wurtzite nanoparticles at low temperatures. On the other hand, the peak shape can give some hints about the nanometric habitus: the annealing temperature should reasonably have led to bigger particles and an increased crystalline fraction, as suggested by the narrow FWHM reported for ZnO nitrate with respect to ZnO Acetate, where larger FWHM values are reasonably ascribable to small crystallites and amorphous nature. Verification in this sense was carried out by calculating the mean crystallite size according to the Scherrer equation (Equation (5)); results are reported in Table 1:

Table 1. Mean crystallite size obtained from the Scherrer equation applied to the first seven crystallographic peaks of investigated samples.

Sample	Mean Crystallite Size
ZnO Acetate route	6.84 ± 1.18 nm
ZnO Commercial	29.85 ± 2.59 nm
ZnO Nitrate (heat-treated) route	24.48 ± 2.09 nm

These data seem to confirm expectations, with the crystallite size of the Acetate sample being about three times lower than the Nitrate (heat-treated) one, which instead has a dimensional range in line with the commercial sample. This is in good agreement with the literature, where other studies report that ZnO dimensions increase proportionally to the increase in annealing temperature [33].

The hydrodynamic behavior of the powdered samples was investigated by means of DLS analysis (Figure 2), in order to evaluate the aggregates' size in an aqueous medium and the colloidal stability of the particles.

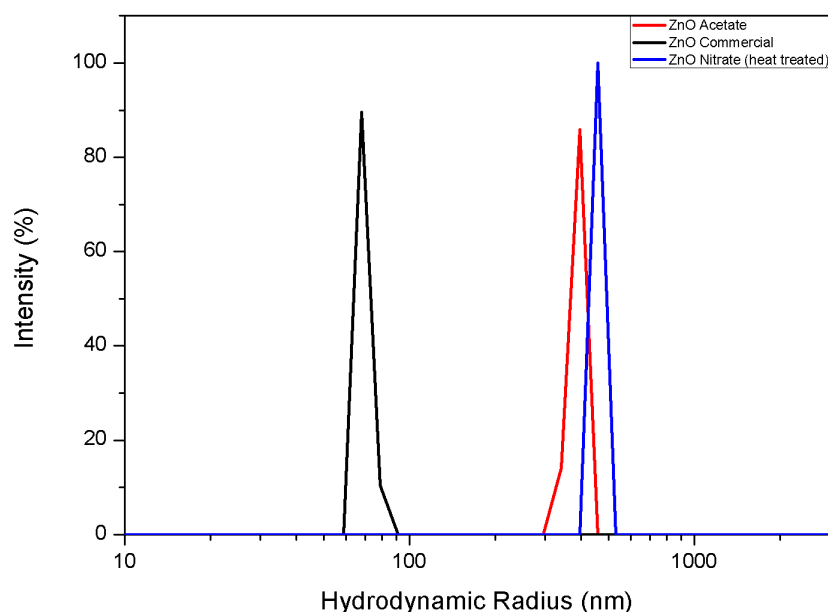
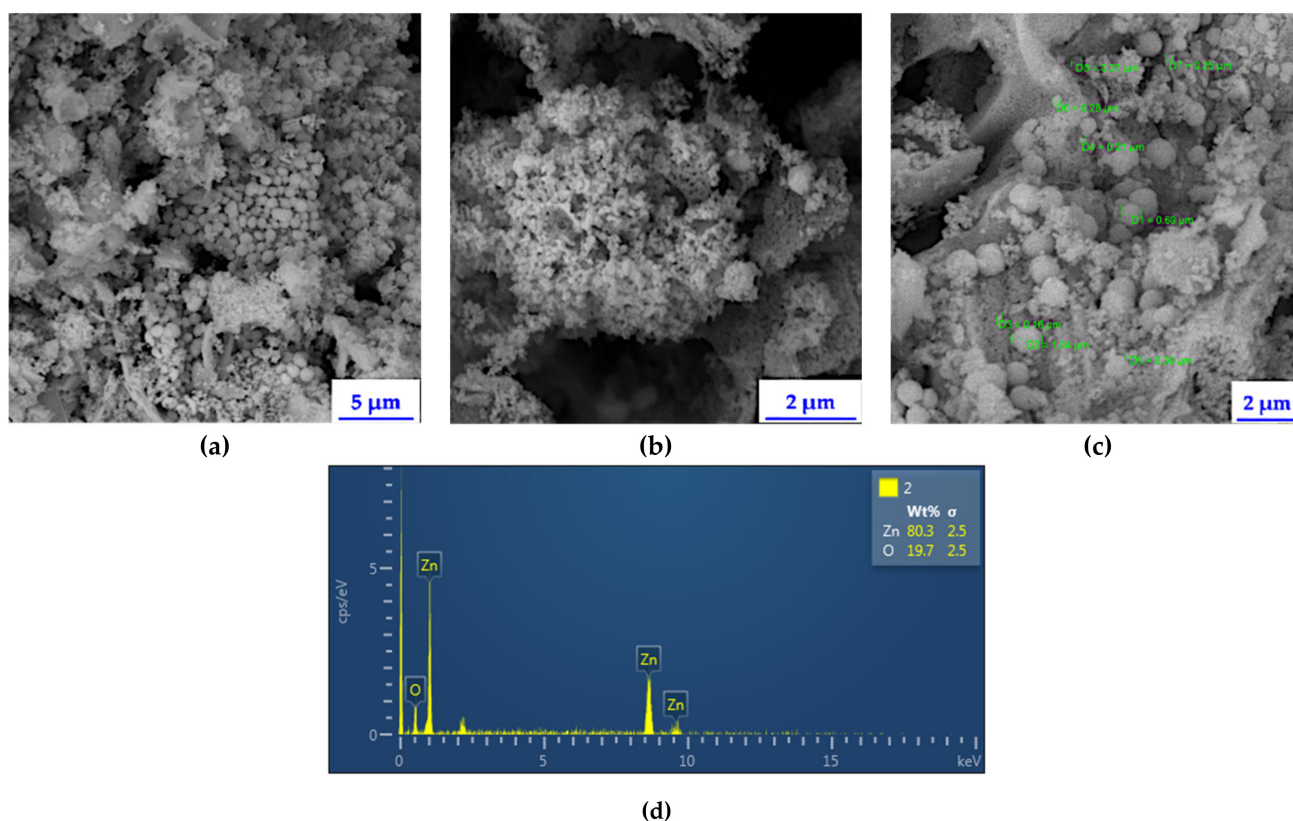


Figure 2. DLS results on the hydrodynamic radius of ZnO samples: ZnO Acetate route (red), ZnO commercial (black), and ZnO Nitrate route (blue).

From the comparison with the data in Table 1, the hydrodynamic radius results are much higher than the crystallite size for all synthesized samples. This suggests that synthesized NPs gather together in aqueous media, in aggregates ranging from 400 to 700 nm. A different consideration applies to the ZnO Commercial sample, whose hydrodynamic radius strongly resembles the crystallite size found with the Scherrer equation. This is probably ascribable to the controlled industrial production process, which leads to homogeneously mono-dispersed NPs. As examined samples were not grafted with any capping agent, the global behavior in water suspension resulted similarly in a short-term period, while the longer-term stability, evaluated along 50 min (equal to the photocatalytic experiments' time, described in Section 3.3), without stirring, resulted quite differently. ZnO Commercial and ZnO Nitrate samples were still visibly dispersed (a whitish aspect of the solution) while ZnO acetate completely settled down. The instability of ZnO Acetate in an aqueous medium can be related to the remarks of Sun et al. [31], which report ZnO to be stable in methanol and hexane solutions rather than aqueous ones.

By means of SEM-EDS characterization, it was possible to address the final morphology and the overall dimensions of ZnO samples to the specific synthetic path investigated. Figure 3a–d shows the morphology of the ZnO Nitrate sample and Figure 4a–c displays the outcome of the ZnO Acetate sample. ZnO Commercial and ZnO Nitrate (not treated) were not analyzed.



dimensions of hundreds of nanometers (160 nm–690 nm), and the DLS results are in line with expectations, highlighting the desired morphology with respect to the thermally untreated sample. The ZnO Acetate sample, synthesized without the annealing process, led instead to a peculiar platelet arrangement: randomly distributed, with sharp nanometric edges, a few micrometers long. This morphological outcome could be reasonably ascribed to the particular ultrasonic bath employed during the synthetic process, in concurrence with the low temperature (63 °C) used during the synthesis.

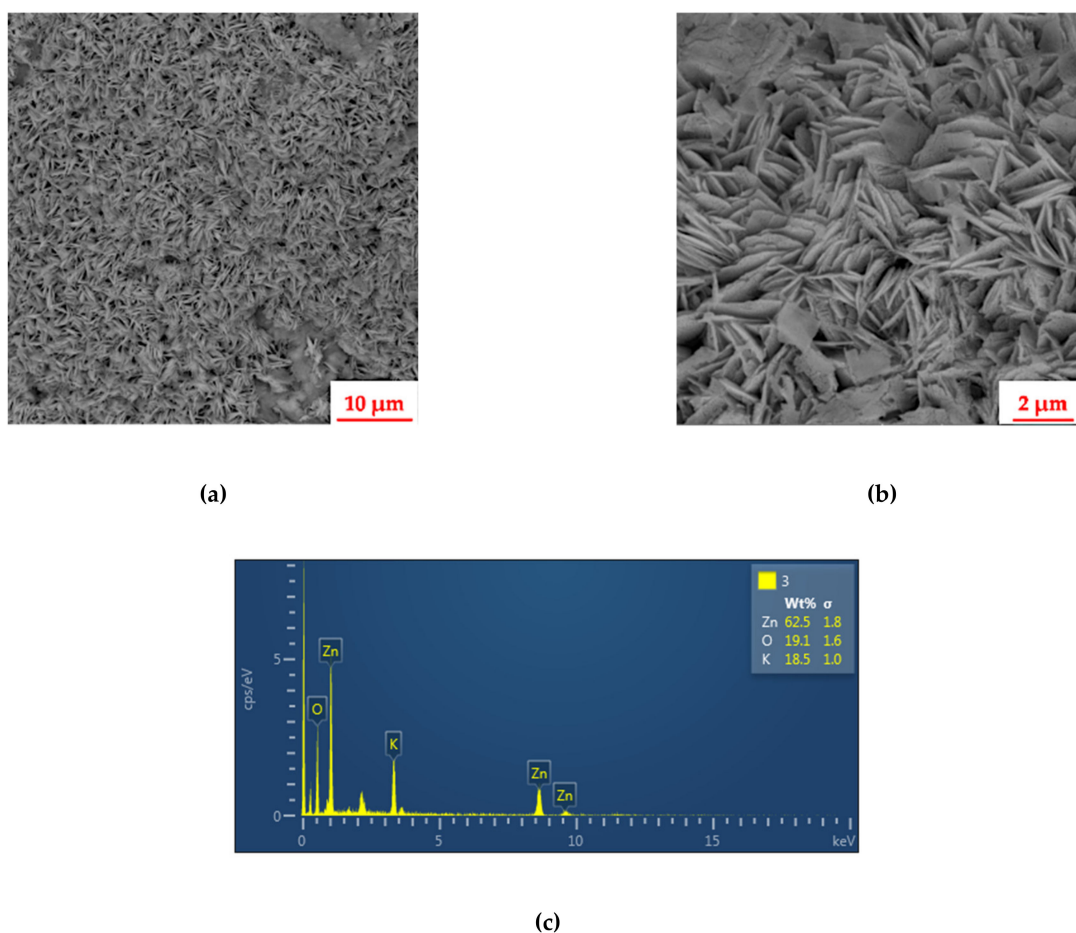


Figure 4. SEM images of ZnO Acetate sample: (a) 5000× magnification (10 μm marker); (b) 20,000× magnification (2 μm marker); (c) EDS elemental composition.

In view of the possible use of the synthesized ZnO nanoparticles in wastewater treatment processes, it is more likely for the spherical nanoparticles to be better photocatalysts, as the spherical shape can exhibit a wider surface area with respect to other shapes. In order to prove this scenario and correlate the highlighted physico-chemical features, preliminary photocatalytic experiments under simulated solar light were performed.

2.2. Photocatalytic Results

Preliminary methylene blue (MB) degradation experiments allowed us to compare the behavior of the different ZnO samples as heterogeneous photocatalysts to find out the most active sample to be used for real applications. Table 2 reports the percentage MB degradation calculated after 50 min of simulated solar light irradiation, and the computed kinetic constants for MB degradation, calculated assuming a 1st order kinetic, as widely reported in the literature [39]. It has to be noted that the constants are computed according to the whole process and thus they must be considered as averages.

Table 2. Photocatalytic results expressed as methylene blue (MB) percentage degradation after 50 min and 1st order kinetic constants.

Samples	MB Dark Absorption (20 min)	MB% Degradation	Dev. st. (n = 3)	k (l)
MB Photolysis	n.c.	8%	2.5	0.002 min ⁻¹
ZnO Acetate route	0.9%	78%	2.0	0.054 min ⁻¹
ZnO Commercial	5.2%	100%*	0.5	0.162 min ⁻¹
ZnO Nitrate (heat treated) route	2.3%	93%	0.9	0.085 min ⁻¹

* 100% Degradation is referred to as MB absorbance lower than the detection limit (DL)

According to the experimental results, the ZnO Commercial sample is able to degrade MB dye down to the detection limit (DL), corresponding to zero absorbance (0.1 ppm) and equivalent to 100% degradation, with the highest kinetic constant, while the two synthetic samples fail to achieve such performances, clearly placing both synthesized products below the commercial one in general terms. Indeed, a difference in MB% degradation up to 15% is observed in the worst case (ZnO Acetate), which is slight but still significant.

However, the results obtained are actually fully in line with the most recent investigations, when it comes to homemade synthesized ZnO.

In a recent work by Rambabu et al. [40], where commercial ZnO was not considered, ZnO catalysts self-produced under conditions similar to the present experimentation recorded MB degradation of about 55–65% in 50 min, therefore below the results obtained here. Furthermore, on the closer comparison, it appears that in [40] the initial concentration of MB was actually half of that used in the present study. In view of this, it is evident that there is still room for improvement and the possibility of modifications to be investigated in the synthesis processes considered.

In order to examine the results in depth, the degradation due to only MB photolysis and MB absorption in dark conditions was also considered and reported in Table 2. However, because of the duration of the experiments, MB was degraded at a maximum of 8% in the considered conditions, which is significantly lower than the overall reached percentages; similarly, the dark absorption, performed in order to understand the surface behavior of the samples, did not exceed 5.2%, which was as low as the photolysis percentage.

Based on these results, it is possible to attribute the degradation of the dye to the photocatalytic activity under solar radiation of the synthesized samples, as a consequence of the semiconductor nature of the material and the physico-chemical features given by the investigated syntheses.

The main differences found in the performance of the samples obtained from the two synthesis paths considered are probably to be sought in the enhanced porosity of the ZnO Nitrate sample, as suggested from SEM images, along with its spherical shape, which can ensure better interaction with the dye with respect to other shapes. In addition, the expected presence of vacancies and crystal defects, imparted by the annealing process to the ZnO lattice, is expected to provide the best catalytic performance for oxidizing/reducing reactions, as also reported in the literature [41]; the preliminary experimental evidence obtained from these photocatalytic results seems to confirm this trend.

As a conclusion, in order to understand and justify the exhibited photocatalytic behavior, diffuse reflectance spectra were recorded to obtain the Energy Gap values (E_{gap}) of the investigated samples. By means of the integrating sphere, it was possible to record percentage Reflectance values on powders in a short spectral range, between 400 and 700 nm. Results were modeled according to the Kubelka-Munk method, based on the following equation:

$$F(R) = \frac{(1 - R)^2}{2R} \quad (1)$$

E_{gap} values were retrieved by the graphical representation of the Tauc Plot, obtained by plotting $(F(R)h\nu)^n$ vs $h\nu$, using $n = 1/2$ for a direct allowed transition, as reported

in [42]. As a consequence of the short spectral range that the exploited instrument could investigate, only the E_{gap} values are reported and shown in Table 3.

Table 3. E_{gap} values obtained from the graphical representation of the Tauc Plot. Values were extrapolated from the slopes in the flat section to $y = 0$.

Samples	E_{gap} Values	λ Absorption
ZnO Nitrate (heat treated) route	3.27 eV	379 nm
ZnO Commercial	3.40 eV	364 nm
ZnO Acetate route	3.31 eV	374 nm

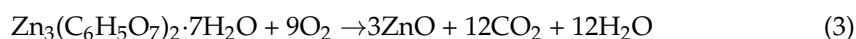
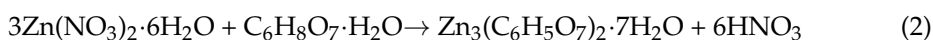
As expected, some differences in the electronic structure were identified: the highest band gap value was recorded for the ZnO Commercial sample, while ZnO Acetate and ZnO Nitrate, differing with the commercial sample, showed a difference of 0.04 eV, equal to a 5 nm difference for photon absorption. These findings are in good agreement with the experimental results highlighted by Zak et al. [34], showing that ZnO E_{gap} should decrease as the annealing temperature increases, while the presence of possible impurities may have affected synthesized ZnO microstructures, lowering the E_{gap} but affecting their photo-activity.

3. Materials and Methods

3.1. ZnO Syntheses

3.1.1. $\text{Zn}(\text{NO}_3)_2 \cdot 6\text{H}_2\text{O}$ Precursor

The following synthetic path was retrieved from the work of Acosta-Humánez et al., where a sol-gel synthesis involving zinc nitrate hexahydrate as a precursor and an annealing post-treatment to reach the Wurtzite phase was investigated [20]. A mass of 5.85 g of $\text{Zn}(\text{NO}_3)_2 \cdot 6\text{H}_2\text{O}$ (98%, Sigma Aldrich, Darmstadt, Germany) was dissolved in 3.4 mL of deionized water (system ARIOSO Water Purification System) while 4.13 g of citric acid monohydrated (99.5+%, Alfa Aesar, Kandel, Germany) was dissolved in 2.5 mL of deionized water. Both solutions were heated up to 70 °C and kept under magnetic stirring for 30 min separately. After this time, zinc nitrate solution was slowly poured into the citric acid solution while kept under stirring, and the reaction mixture was kept in the same stirring and temperature conditions until gel formation. The gel was then transferred into a porcelain capsule and left to dry for 12 h at 100 °C. The resulting xerogel was roughly ground in an agate mortar to obtain the powder of zinc citrate which was eventually heat treated in a muffle furnace at 500 °C for 12 h to obtain the desired crystalline product. The overall reactions can be described as follows:



3.1.2. $\text{Zn}(\text{CH}_3\text{COOH})_2$ Precursor

The following solvothermal route was retrieved from the work of Lova et al. [43] as Wurtzite ZnO without an annealing process was reported to be obtained. A mass of 4.61 g of zinc acetate (99.99%, Sigma Aldrich, Darmstadt, Germany) was dissolved in 200 mL of methanol (99.8%, Scharlab S.L., Sentmenat, Spain), which was in turn placed in a three-neck round-bottom flask and left in a thermostated ultrasonic bath at 63 °C in reflux conditions. Separately, 2.35 g of potassium hydroxide (Merck, p.a., Darmstadt, Germany) was dissolved in 100 mL of methanol and the resulting solution was added dropwise in the first reaction system. After 3 h, a white precipitate was visible at the bottom of the flask; it was left to settle down while the supernatant was removed and the leftover was washed with a methanol/water solution. Settling washing cycles were repeated four times and

eventually the product was dried in an oven at 100 °C for 12 h. The overall reaction can be described as follows:



3.2. Characterization Techniques

XRD spectra on synthesized samples were recorded with the powders method, by means of an automatic diffractometer Empyrean (Malvern PANalytical, Malvern, United Kingdom) in Bragg-Brentano ($\theta:2\theta$) geometry, using a two-axis high-resolution vertical goniometer. A 1.8 kW Cu $K\alpha$ sealed ceramic tube with a Ni filter was used as an X-ray source. Spectra were acquired from 20 to 80 (2θ), using 0.02 (2θ) as the step size and 4 s as the time per step. Crystallite mean size was retrieved on measured XRD spectra using the Scherrer equation:

$$D = \frac{K\lambda}{\beta \cos \theta} \quad (5)$$

where D represents crystallite mean size, K is the Scherrer constant (equal to approximately 0.9), λ is the X-ray wavelength used, b is the full width at half maximum of diffraction peaks, and q is the peak position.

DLS analysis was performed with a zetasizer Nano ZS90 (Malvern Instruments, Malvern, United Kingdom), where 0.01 wt% (10 mg/mL) aqueous suspensions of the synthesized nanoparticle were subjected to the characterization. The wavelength of the laser used was 632.8 nm so that it was possible to put 0.000 as the absorption. Refractive Index (R.I.) for the dispersant medium (water) was set to 1.33 while R.I. for ZnO was set to 2.263. Mild centrifugation followed by sonication with Omni Sonic Ruptor Ultrasonic Homogenizer (tip microprocessor 5/3200, at 40% power) was performed before analysis, to remove bigger aggregates. Measurements were performed at 25 °C thermostated temperature by means of a Peltier thermostated system.

SEM images were acquired with a FeSEM Zeiss SUPRA 40VP microscope (Carl Zeiss AG, Oberkochen, Germany) coupled with an EDS detector (EDXS Oxford "INCA Energie 450 x 3" Oxford Instrument, Abingdon UK) for micro-analysis. The experimental conditions were set at low voltage (5 kV). A second SEM (Tescan Vega3 XML) coupled with an EDS detector (Oxford X-Max) and software (AZtec 2.4) was also employed. Samples were prepared with Au coating.

Diffuse reflectance spectra were collected by means of a CM-2600D spectrophotometer (Konica Minolta, Tokyo, Japan), equipped with an integrating sphere. DRS spectra were recorded in the spectral range between 400 and 700 nm (the instrument does not allow the investigation in a shorter wavelength range) to extrapolate the E_{gap} values of investigated samples through graphical extrapolation from the Tauc plot, obtained using the Kubelka-Munk method [42].

3.3. Photocatalytic Experiments

Photocatalytic experiments were performed in order to preliminarily investigate the activity of the synthesized nanoparticles and to identify any difference ascribable to the synthesis. A volume of 25 mL of a 0.02 g/L MB aqueous solution, in the presence of suspended ZnO NPs, at a concentration of 0.5 mg/mL, was subjected to solar simulated light irradiation with an OSRAM Ultra-Vitalux lamp (300 W). MB dye was chosen as suggested by the ISO 10678:2010 protocol, for the assessment of heterogeneous photocatalysts activity in aqueous solutions. The lamp's emission spectrum is depicted in Figure 5 while its irradiance is reported in the literature to be: 1.1 W/m² for UV-B range, 7.3 W/m² for UV-A range, and 29.7 W/m² for Vis range (these values take the lifetime of the lamps used into account) [44]. In order to overcome the intensity decrease due to their lifetime, lamps were put at 20 cm distance from the solutions. Suspended samples were kept under magnetic stirring in the dark for 20 min in order to ensure the adsorption/desorption equilibrium between the photocatalyst and the dye, as a result of dark absorption experiments, per-

formed with the same conditions but without irradiation. Eventually, the photocatalytic experiments were left under irradiation for another 50 min (experiments were performed in triplicate). Aliquots withdrawn from the solution were subjected to 13,200 rpm centrifugation and eventually analyzed by means of UV-Vis spectrophotometry (LAMBDA 35 Perkin-Elmer-Whaltam, MA, USA) to calculate the percentage MB abatement. Recovery and recycling experiments were not reported as they are the result of ongoing scientific collaboration and are meant to be delivered successively. The quant mode was used to observe the absorbance value recorded for each aliquot at 664 nm, which corresponds to the maximum absorption value of methylene blue.

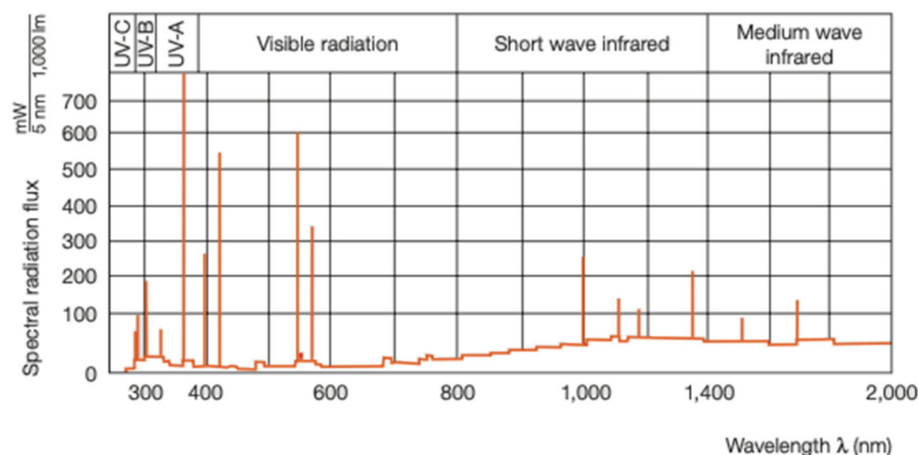


Figure 5. Spectral distribution of the OSRAM Ultra-Vitalux 300W lamp used. Reprinted with permission from ref. [45]. Copyright 2019 Elsevier and Copyright Clearance Center.

4. Conclusions

In the present work, two different synthetic paths for the synthesis of ZnO nanoparticles to be addressed for use in the environmental field of wastewater remediation were analyzed and compared. By means of a physico-chemical characterization, along with a preliminary kinetic evaluation of the photocatalytic performances, it was possible to determine the most important parameters that ZnO nanoparticles should possess to exhibit good photocatalytic activity to be used in the pollutants' degradation in water media.

After the experimental investigation, it was shown that the Wurtzite crystalline phase alone is not sufficient to reach the desired photocatalytic activity, but rather the annealing process results in a crucial parameter for the synthesis of efficient zinc oxide. Other studies report that temperature directly affects the electronic behavior and the lattice nature of the semiconductor, and the present experimentation suggests this as a key parameter to get the correct lattice features for photocatalytic water treatment. Indeed, the absence of the annealing procedure for the ZnO Acetate sample, as highlighted by XRD, led to a reduced crystalline fraction and likely led to a reduced lattice arrangement of defects and vacancies (acting as active sites for interaction and charge transfer in the heterogeneous photocatalytic process), resulting in reduced degradation of the target contaminant.

Unfortunately, none of the synthesized samples were able to reach the performance of ZnO Commercial sample: even though it was not the desired outcome, the syntheses prepared proved to be quite efficient, with results in line with or superior to those reported in the literature for other self-produced ZnO NPs. Although further investigation is needed, it's reasonable to attribute this outcome to a sum of influences resulting from the industrial procedure (not fully disclosed), which made the ZnO Commercial sample highly compatible with pollutants.

Regarding this, it is worth noting that, for research purposes, a synthetic route is much more desirable than a commercial product. Especially when dealing with environmental remediation, the perspective of a possible recovery of resources for in-house production, and the sustainability of the remediation materials and processes themselves, are remarkable

aspects in line with all the most recent directives of the European Community on the circular economy and zero waste approaches. In addition, dealing with homemade synthesis simplifies the coupling with other active materials for enhanced activity. Reassessing the results obtained in the light of these considerations, and therefore excluding the commercial ZnO from the comparison, the most suitable synthetic path to obtain ZnO for wastewater application appears to be the Nitrate route, due to the lower E_{gap} , the spherical shape, and the colloidal stability in water, and also considering the crystallinity and purity of the sample, as shown by the characterizations performed. On the contrary, the Acetate route led to a particular platelet arrangement of ZnO nanoparticles, but their stability resulted unfavorably for aqueous solutions, limiting their use in environmental applications.

Future perspectives could involve the performance of further characterization techniques (e.g., BET measurements) in an attempt to fully identify the synthetic parameters that can confer the ZnO Commercial sample's photocatalytic features while preserving and improving the environmental sustainability of the presented summary. At the same time, tests are planned concerning real applications (such as real pollutants, volume scale-up, recovery, and recycling of the photocatalyst).

Author Contributions: conceptualization, S.A., I.B.; methodology S.A.; validation S.A.; investigation, S.A., I.B.; resources, M.F.; data curation, S.A., I.B.; writing—original draft preparation, S.A.; writing—review and editing, S.A., M.V., M.F.; visualization, M.V.; supervision, M.V., M.F.; project administration, M.F.; funding acquisition, M.F. All authors have read and agreed to the published version of the manuscript.

Funding: Some of the researchers who worked on the present paper are financed by the Operating Program Por-FSE Regione Liguria 2014-2020 (Grant number RLOF18ASSRIC/32).

Data Availability Statement: Data is contained within the article.

Acknowledgments: Authors would like to acknowledge Emanuela Sartori (Univ. of Genoa, Italy) for her precious help in the collection of XRD patterns.

Conflicts of Interest: The authors declare no conflict of interest.

References

1. Pietrelli, L.; Ferro, S.; Reverberi, A.P.; Vocciante, M. Removal and recovery of heavy metals from tannery sludge subjected to plasma pyro-gasification process. *J. Clean. Prod.* **2020**, *273*, 123166. [[CrossRef](#)]
2. Soltani, R.D.C.; Jorfi, S.; Safari, M.; Rajaei, M.S. Enhanced sonocatalysis of textile wastewater using bentonite-supported ZnO nanoparticles: Response surface methodological approach. *J. Environ. Manag.* **2016**, *179*, 47–57. [[CrossRef](#)]
3. Vocciante, M.; Finocchi, A.; De Folly D'Auris, A.; Conte, A.; Tonziello, J.; Pola, A.; Reverberi, A.P. Enhanced oil spill remediation by adsorption with interlinked multilayered graphene. *Materials* **2019**, *12*, 2231. [[CrossRef](#)]
4. Fu, F.; Wang, Q. Removal of heavy metal ions from wastewaters: A review. *J. Environ. Manag.* **2011**, *92*, 407–418. [[CrossRef](#)] [[PubMed](#)]
5. Vocciante, M.; De Folly D'Auris, A.; Finocchi, A.; Tagliabue, M.; Bellettato, M.; Ferrucci, A.; Reverberi, A.P.; Ferro, S. Adsorption of ammonium on clinoptilolite in presence of competing cations: Investigation on groundwater remediation. *J. Clean. Prod.* **2018**, *198*, 480–487. [[CrossRef](#)]
6. Pietrelli, L.; Ippolito, N.M.; Ferro, S.; Dovì, V.G.; Vocciante, M. Removal of Mn and As from drinking water by red mud and pyrolusite. *J. Environ. Manag.* **2019**, *237*, 526–533. [[CrossRef](#)]
7. Bel Hadjtaiefa, H.; Ben Zina, M.; Galvez, M.E.; Da Costa, P. Photocatalytic degradation of methyl green dye in aqueous solution over natural clay-supported ZnO-TiO₂ catalysts. *J. Photochem. Photobiol. A Chem.* **2016**, *315*, 25–33. [[CrossRef](#)]
8. Bloh, J.Z.; Dillert, R.; Bahnemann, D.W. Designing Optimal Metal-Doped Photocatalysts: Correlation between Photocatalytic Activity, Doping Ratio, and Particle Size. *J. Phys. Chem. C* **2012**, *116*, 25558–25562. [[CrossRef](#)]
9. De Franco, M.A.E.; da Silva, W.L.; Bagnara, M.; Lansarin, M.A.; dos Santos, J.H.Z. Photocatalytic degradation of nicotine in an aqueous solution using unconventional supported catalysts and commercial ZnO/TiO₂ under ultraviolet irradiation. *Sci. Total Environ.* **2014**, *494*, 97–103. [[CrossRef](#)]
10. Toccafondi, C.; Dante, S.; Reverberi, A.P.; Salerno, M. Biomedical Applications of Anodic Porous Alumina. *Curr. Nanosci.* **2015**, *11*, 572–580. [[CrossRef](#)]
11. Pascariu, V.; Avadanei, O.; Gasner, P.; Stoica, I.; Reverberi, A.P.; Mitoseriu, L. Preparation and characterization of PbTiO₃-epoxy resin compositionally graded thick films. *Phase Transit.* **2013**, *86*, 715–725. [[CrossRef](#)]
12. McCluskey, M.; Jokela, S. Sources of n-type conductivity in ZnO. *Phys. B Condens. Matter* **2007**, *401*, 355–357. [[CrossRef](#)]

13. Jiang, Y.; O'Neill, A.J.; Ding, Y. Zinc oxide nanoparticle-coated films: Fabrication, characterization, and antibacterial properties. *J. Nanoparticle Res.* **2015**, *17*, 180. [[CrossRef](#)]
14. Van de Walle, C.G. Hydrogen as a cause of doping in zinc oxide. *Phys. Rev. Lett.* **2000**, *85*, 1012–1015. [[CrossRef](#)] [[PubMed](#)]
15. Janotti, A.; Van de Walle, C.G. Fundamentals of zinc oxide as a semiconductor. *Rep. Prog. Phys.* **2009**, *72*, 1–29. [[CrossRef](#)]
16. Reverberi, A.P.; Salerno, M.; Lauciello, S.; Fabiano, B. Synthesis of copper nanoparticles in ethylene glycol by chemical reduction with vanadium (+2) salts. *Materials* **2016**, *9*, 809. [[CrossRef](#)]
17. Janotti, A.; Van de Walle, C.G. Hydrogen multicentre bonds. *Nat. Mater.* **2007**, *6*, 44–47. [[CrossRef](#)] [[PubMed](#)]
18. Martinelli, A.; Alberti, S.; Caratto, V.; Lova, P.; Locardi, F.; Pampararo, G.; Villa, S.; Ferretti, M. Structural studies on copper and nitrogen doped nanosized anatase. *Z. Krist. Cryst. Mater.* **2018**, *233*, 867–876. [[CrossRef](#)]
19. Caratto, V.; Locardi, F.; Alberti, S.; Villa, S.; Sanguineti, E.; Martinelli, A.; Balbi, T.; Canesi, L.; Ferretti, M. Different sol–gel preparations of iron-doped TiO₂ nanoparticles: Characterization, photocatalytic activity and cytotoxicity. *J. Sol Gel Sci. Technol.* **2016**, *80*, 152–159. [[CrossRef](#)]
20. Humánez, M.F.A.; Vides, L.A.M.; Almanza-Montero, O.A. Sol-gel synthesis of zinc oxide nanoparticle at three different temperatures and its characterization via XRD, IR and EPR. *DYNA* **2016**, *83*, 224–228. [[CrossRef](#)]
21. Alberti, S.; Ferretti, M.; Vicini, S.; Castellano, M.; Caratto, V. Porous polydimethylsiloxane membranes loaded with low-temperature crystallized TiO₂ NPs for detachable antibacterial films. *J. Mater. Sci.* **2018**, *54*, 1665–1676. [[CrossRef](#)]
22. Alberti, S.; Locardi, F.; Sturini, M.; Speltini, A.; Maraschi, F.; Costa, G.A.; Ferretti, M.; Caratto, V. Photocatalysis in darkness: Optimization of sol-gel synthesis of NP-TiO₂ supported on a persistent luminescence material and its application for the removal of ofloxacin from water. *J. Nanomed. Nanotechnol.* **2018**, *9*, 501. [[CrossRef](#)]
23. Alberti, S.; Caratto, V.; Peddis, D.; Belviso, C.; Ferretti, M. Synthesis and characterization of a new photocatalyst based on TiO₂ nanoparticles supported on a magnetic zeolite obtained from iron and steel industrial waste. *J. Alloys Compd.* **2019**, *797*, 820–825. [[CrossRef](#)]
24. Sampaio, M.J.; Bacsa, R.; Benyounes, A.; Axet, R.; Serp, P.; Silva, C.; Silva, A.; Faria, J. Synergistic effect between carbon nanomaterials and ZnO for photocatalytic water decontamination. *J. Catal.* **2015**, *331*, 172–180. [[CrossRef](#)]
25. Kumar, P.P.N.V.; Shameem, U.; Kollu, P.; Kalyani, R.L.; Pammi, S.V.N. Green Synthesis of Copper Oxide Nanoparticles Using Aloe vera Leaf Extract and Its Antibacterial Activity Against Fish Bacterial Pathogens. *BioNanoScience* **2015**, *5*, 135–139. [[CrossRef](#)]
26. Senthilkumar, S.R.; Sivakumar, T. Green tea (*Camelia Sinensis*) mediated synthesis of zinc oxide (ZnO) nanoparticles and studies on their antimicrobial activities. *Int. J. Pharm. Pharm. Sci.* **2014**, *6*, 461–465.
27. Balasooriya, E.R.; Jayasinghe, C.D.; Jayawardena, U.A.; Ruwanthika, R.W.D.; Mendis de Silva, R.; Udagama, P.V. Honey mediated green synthesis of nanoparticles: New era of safe technology. *Hindawi J. Nanomater.* **2017**, 5919836. [[CrossRef](#)]
28. Azizi, S.; Ahmad, M.B.; Namvar, F.; Mohamad, R. Green biosynthesis and characterization of zinc oxide nanoparticles using brown marine macroalga *Sargassum muticum* aqueous extract. *Mater. Lett.* **2014**, *116*, 275–277. [[CrossRef](#)]
29. Fardood, S.T.; Ramazani, A.; Moradi, S.; Asiabi, P.A. Green synthesis of zinc oxide nanoparticles using arabic gum and photocatalytic degradation of direct blue 129 dye under visible light. *J. Mater. Sci. Mater. Electron.* **2017**, *28*, 13596–13601. [[CrossRef](#)]
30. Vigneshwaran, N.; Kumar, S.; A Kathe, A.; Varadarajan, P.V.; Prasad, V. Functional finishing of cotton fabrics using zinc oxide–soluble starch nanocomposites. *Nanotechnology* **2006**, *17*, 5087–5095. [[CrossRef](#)]
31. Sun, D.; Wong, M.; Sun, L.; Li, Y.; Miyatake, N.; Sue, H.-J. Purification and stabilization of colloidal ZnO nanoparticles in methanol. *J. Sol-Gel Sci. Technol.* **2007**, *43*, 237–243. [[CrossRef](#)]
32. Znaidi, L. Sol-gel deposited ZnO thin films: A review. *Mater. Sci. Eng. B* **2010**, *174*, 18–30. [[CrossRef](#)]
33. Xu, L.; Gu, F.; Su, J.; Chen, Y.; Li, X.; Wang, X. The evolution behavior of structures and photoluminescence of K-doped ZnO thin films under different annealing temperatures. *J. Alloys Compd.* **2011**, *509*, 2942–2947. [[CrossRef](#)]
34. Zak, A.K.; Abrishami, M.E.; Majid, W.A.; Yousefi, R.; Hosseini, S. Effects of annealing temperature on some structural and optical properties of ZnO nanoparticles prepared by a modified sol–gel combustion method. *Ceram. Int.* **2011**, *37*, 393–398. [[CrossRef](#)]
35. Villa, S.; Caratto, V.; Locardi, F.; Alberti, S.; Sturini, M.; Speltini, A.; Maraschi, F.; Canepa, F.; Ferretti, M. Enhancement of TiO₂ NPs Activity by Fe₃O₄ Nano-Seeds for Removal of Organic Pollutants in Water. *Materials* **2016**, *9*, 771. [[CrossRef](#)]
36. Alberti, S.; Villa, S.; Singh, G.; Seland, F.; Martinelli, A.; Ferretti, M.; Canepa, F.; Caratto, V. Systematic study on TiO₂ crystallization via hydrothermal synthesis in the presence of different ferrite nanoparticles as nucleation seeds. *J. Nanosci. Nanotechnol.* **2019**, *19*, 4994–4999. [[CrossRef](#)] [[PubMed](#)]
37. Sofianos, V.; Lee, J.; Silvester, D.; Samanta, P.; Paskevicius, M.; English, N.; Buckley, C. Diverse morphologies of zinc oxide nanoparticles and their electrocatalytic performance in hydrogen production. *J. Energy Chem.* **2021**, *56*, 162–170. [[CrossRef](#)]
38. Lee, K.M.; Lai, C.W.; Ngai, K.S.; Juan, J.C. Recent developments of zinc oxide based photocatalyst in water treatment technology: A review. *Water Res.* **2016**, *88*, 428–448. [[CrossRef](#)]
39. Xiong, S.F.; Yin, Z.L.; Yuan, Z.F.; Yan, W.B.; Yang, W.Y.; Liu, J.J.; Zhang, F. Dual frequency (20/40 kHz) ultra-sonic assisted photocatalysis for degradation of methylene blue effluent: Synergistic effect and kinetic study. *Ultrason. Sonochem.* **2012**, *19*, 756–761. [[CrossRef](#)]
40. Rambabu, K.; Bharath, G.; Banat, F.; Show, P.L. Green synthesis of zinc oxide nanoparticles using Phoenix dactylifera waste as bioreductant for effective dye degradation and antibacterial performance in wastewater treatment. *J. Hazard. Mater.* **2021**, *402*, 123560. [[CrossRef](#)]

41. Kurbanov, S.; Yang, W.C.; Kang, T.W. Kelvin probe force microscopy of defects in ZnO nanocrystals associated with emission at 3.31 eV. *Appl. Phys. Express* **2011**, *4*, 021101. [[CrossRef](#)]
42. López, R.; Gómez, R. Band-gap energy estimation from diffuse reflectance measurements on sol–gel and commercial TiO₂: A comparative study. *J. Sol. Gel Sci. Technol.* **2012**, *61*, 1–7. [[CrossRef](#)]
43. Lova, P.; Manfredi, G.; Boarino, L.; Laus, M.; Urbinati, G.; Losco, T.; Marabelli, F.; Caratto, V.; Ferretti, M.; Castellano, M.; et al. Hybrid ZnO:polystyrene nanocomposite for all-polymer photonic crystals. *Phys. Status Solidi C* **2015**, *12*, 158–162. [[CrossRef](#)]
44. Stefan, M. More than just light. Solutions in ultraviolet light. In *100 Years of Innovation Osram*; OSRAM GmbH: Munich, Germany, 2016; p. 24.
45. Mahfoudh, I.; Principi, P.; Fioretti, R.; Safi, M. Experimental studies on the effect of using phase change material in a salinity-gradient solar pond under a solar simulator. *Sol. Energy* **2019**, *186*, 335–346.